Room-Temperature Interfacial Approach Towards Iron/Nitrogen co-Doped Fibrous Porous Carbons as Electrocatalysts for Oxygen Reduction Reaction and Zn-Air Batteries

Chenbao Lu,[a] Jichao Zhang,[e] Zhenying Chen,[a] Kaiyue Jiang,[a] Mingqiang Li,[c] Fan Zhang,[a] Gangsheng Tong,[a] Xiaoxin Zou,[d] Yuezeng Su,*[b] Xiaodong Zhuang*[a]*

Author affiliations:

* Corresponding authors

a State Key Laboratory of Metal Matrix Composites & Shanghai Key Laboratory of Electrical Insulation and Thermal Ageing, School of Chemistry and Chemical Engineering, Shanghai Jiao Tong University, Dongchuan Road 800, Shanghai 200240, China.

E-mail: zhuang@sjtu.edu.cn, fan-zhang@sjtu.edu.cn.

b School of Electronic Information and Electrical Engineering, Shanghai Jiao Tong University, Shanghai 200240, P. R. China.

E-mail: yzsu@sjtu.edu.cn.

c Instrumental analysis center, Shanghai Jiao Tong University, Shanghai 200240, P. R. China.

d State Key Laboratory of Inorganic Synthesis and Preparative Chemistry, College of Chemistry, Jilin University, Changchun 130012, P.R. China

e Shanghai Synchrotron Radiation Facility, Shanghai Advanced Research Institute, Chinese Academy of Sciences, No. 239 Zhangheng Road, Shanghai 201204, China

Experimental

Chemicals

$FeCl_3 \cdot 6H_2O$, polyvinyl alcohol (PVA), Zinc chloride ($ZnCl_2$) and aniline were purchased from Aladdin Reagent Co. Ammonium persulfate (APS), potassium hydroxide (KOH), sulfuric acid (H_2SO_4), hydrochloric acid (HCl, 37 wt.%), and toluene were purchased from Sinopharm Chemical Reagent Co. Commercial Pt/C (20 wt.%) was purchased from Hesen. Nafion solution (5 wt.%) was purchased from DuPont, Ltd.

Characterization.

SEM measurements were performed on a FEI Sirion-200 field emission scanning electron microscope. Transmission electron microscopy (TEM) images were acquired using a Tecnai G2 F20 S-TWIN transmission electron microscope (FEI) operated at 200 kV. XRD analysis was performed on a RigakuD/Max 2500 X-ray diffractometer with Cu Kα radiation (k = 1.54 Å) at a generator voltage of 40 kV and a generator current of 50 mA with a scanning speed of 6° min^{-1} over the range 5−80° (2θ). The Raman spectra of samples were obtained on Lab-RAM HR800 with excitation by an argon ion laser (532 nm). X-ray photoemission spectroscopy (XPS) measurements were performed on a PHI-5000C ESCA system; the C 1s value was set at 284.6 eV for charge corrections. The gas sorption isotherms were measured via an Autosorb-iQA3200-4 sorption analyzer (Quantatech Co., USA) based on N_2 adsorption/desorption.

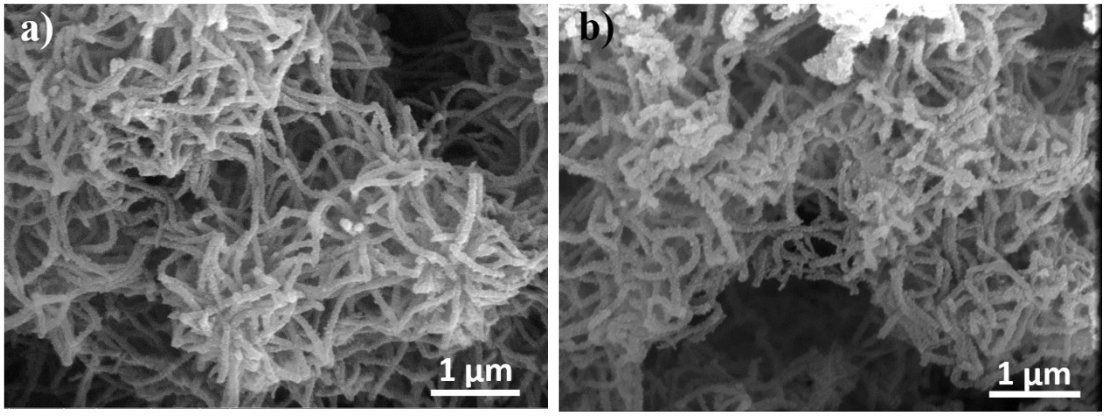

Figure S1. (a) SEM image of Fe@PANI; (b) SEM image of PANI. Both Fe@PANI and PANI show the similar coral-like morphology.

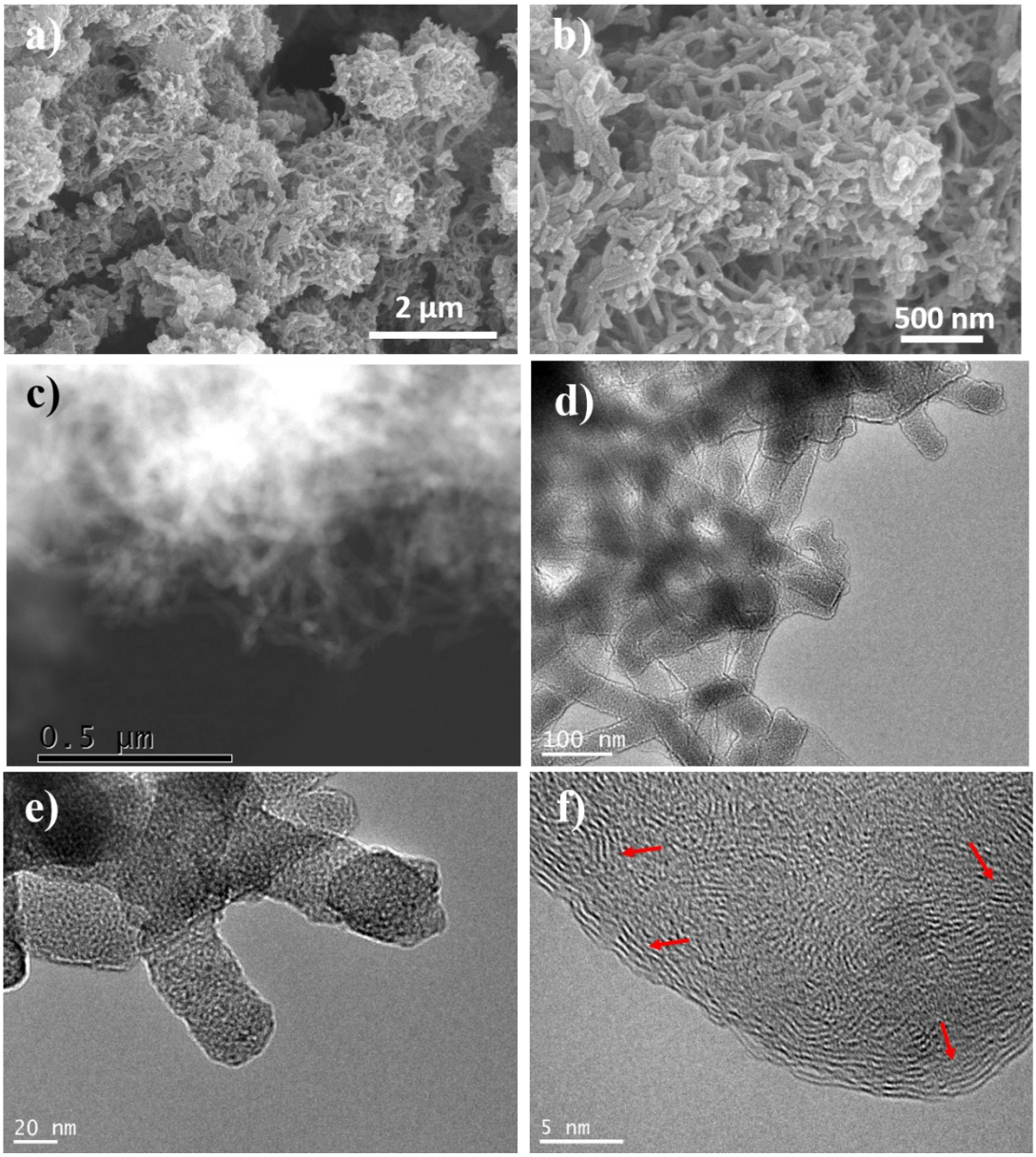

Figure S2. (a) and (b) SEM, (c) and (d) TEM images of Fe/NPCF-900a; (e) and (f) HRTEM images of Fe/NPCF-900a. Similar coral-like morphology can be maintained in a certain extent after carbonization under high temperature. In HRTEM obvious graphitic structure can be detected.

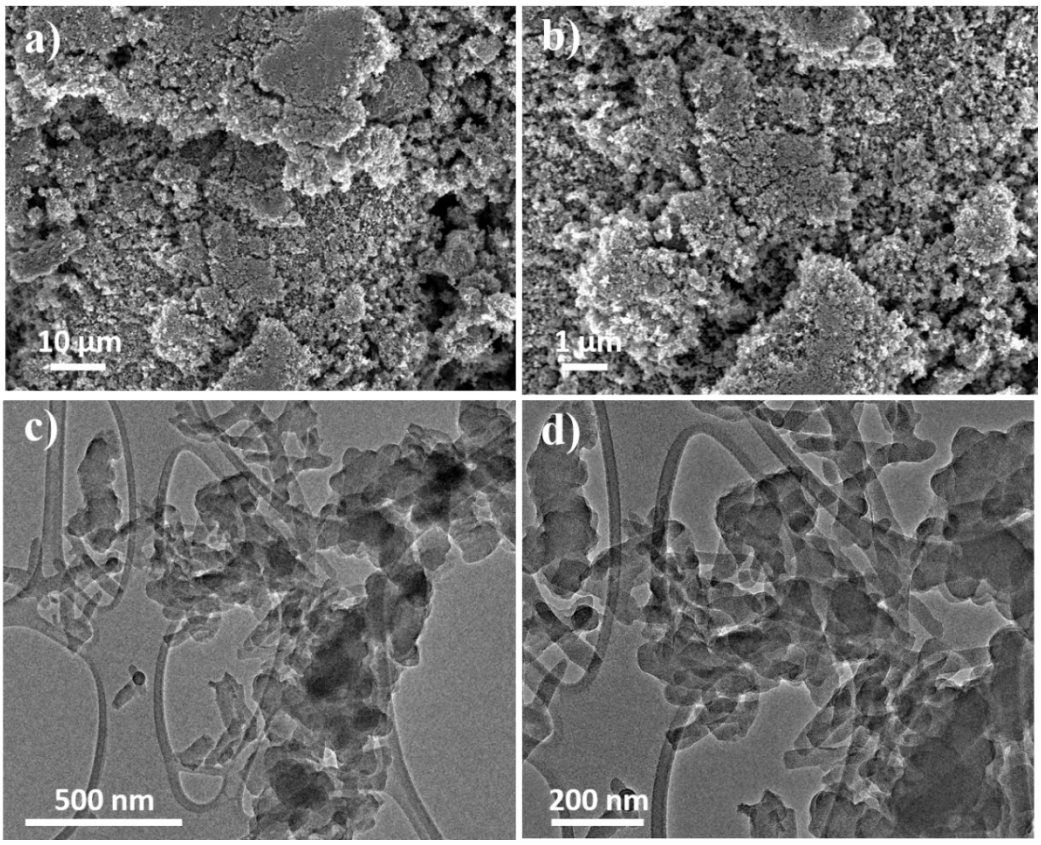

Figure S3. a) and b) SEM images of Fe/NPC; c) and d) TEM images of Fe/NPC prepared by solution polymerization. It can be seen that the materials are irregularly shaped agglomerates.

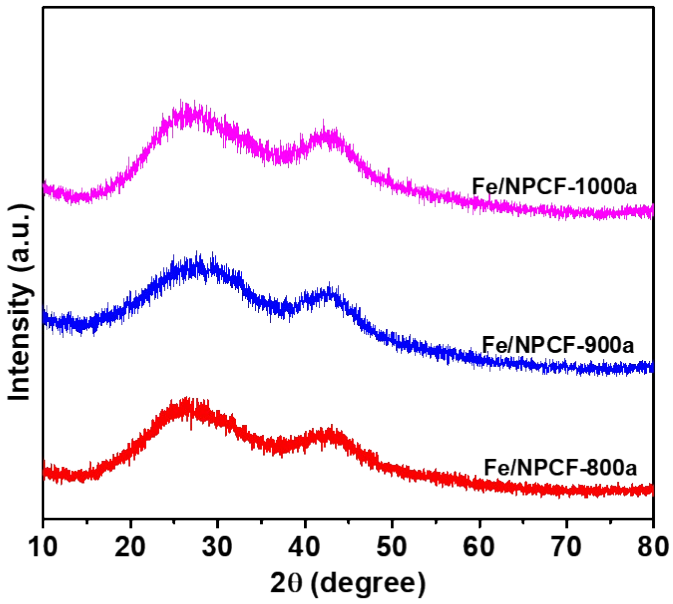

Figure S4. XRD patterns of Fe/NPCF-800a, Fe/NPCF-900a, and Fe/NPCF-1000a. No shape metal and metal composites peaks can be detected.

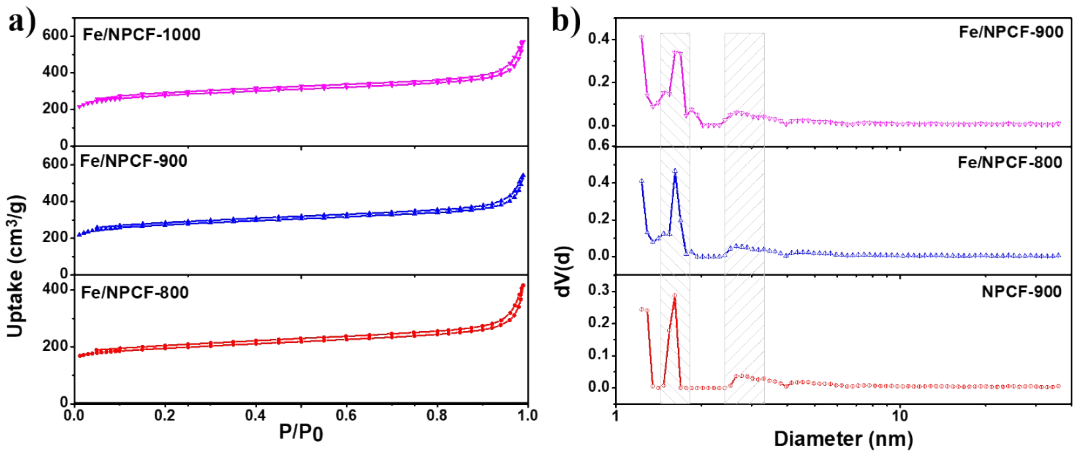

Figure S5. (a) Nitrogen adsorption/desorption isotherms; (b) Corresponding pore size distribution curves calculated by NLDFT method for Fe/NPCF-800, Fe/NPCF-900, and Fe/NPCF-1000. Both obtained materials show the high specific surface area and hierarchal pores structure.

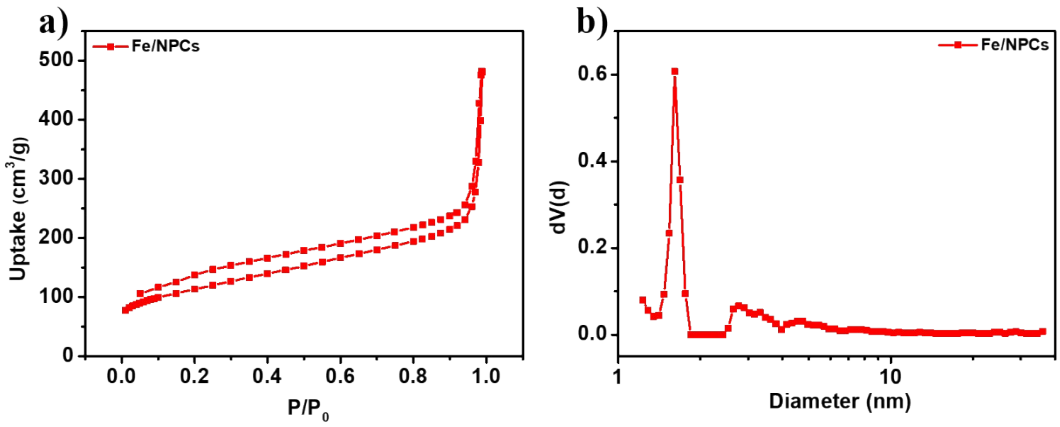

Figure S6. (a) Nitrogen adsorption/desorption isotherms; (b) Corresponding pore size distribution curves calculated by NLDFT method for Fe/NPC prepared by general solution polymerization.

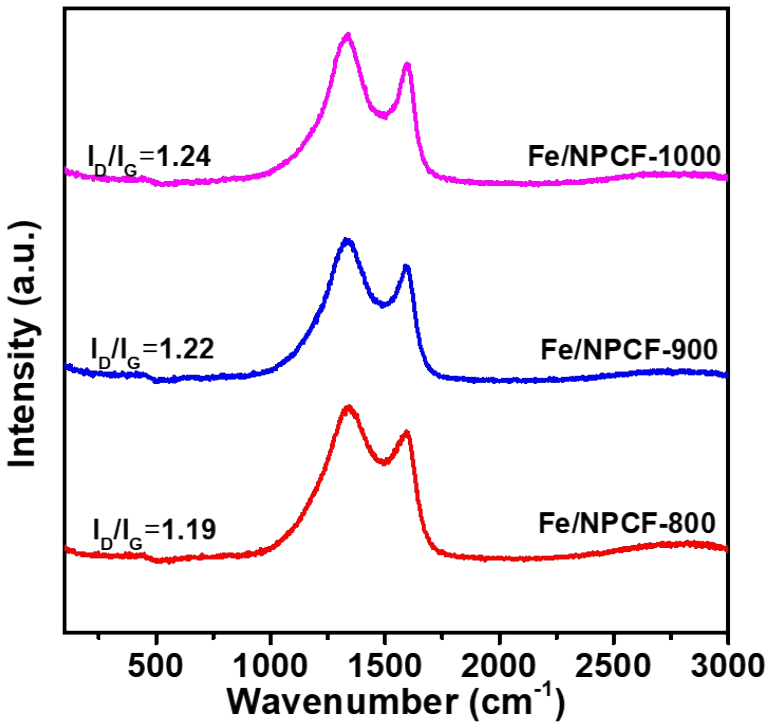

Figure S7. Raman spectra for Fe/NPCF-800, Fe/NPCF-900, and Fe/NPCF-1000. I_D/I_G ratios increased with the raising of pyrolysis temperature, and the materials activation by ammonia show higher values of I_D/I_G, indicating more defective sites have been formed by ammonia etched.

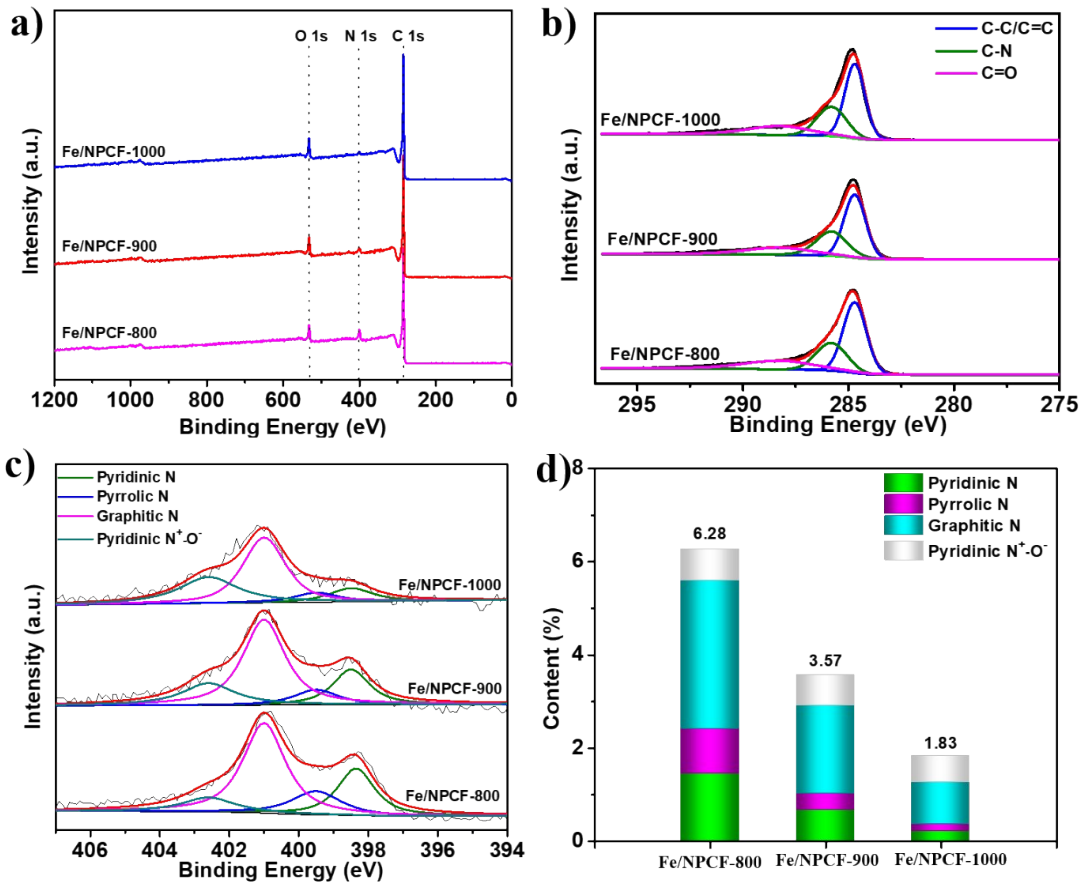

Figure S8. (a) XPS survey spectra; (b) High-resolution C 1s spectra; (c) High-resolution N 1s spectra; and (d) Corresponding nitrogen bonding configurations for Fe/NPCF-800, Fe/NPCF-900, and Fe/NPCF-1000.

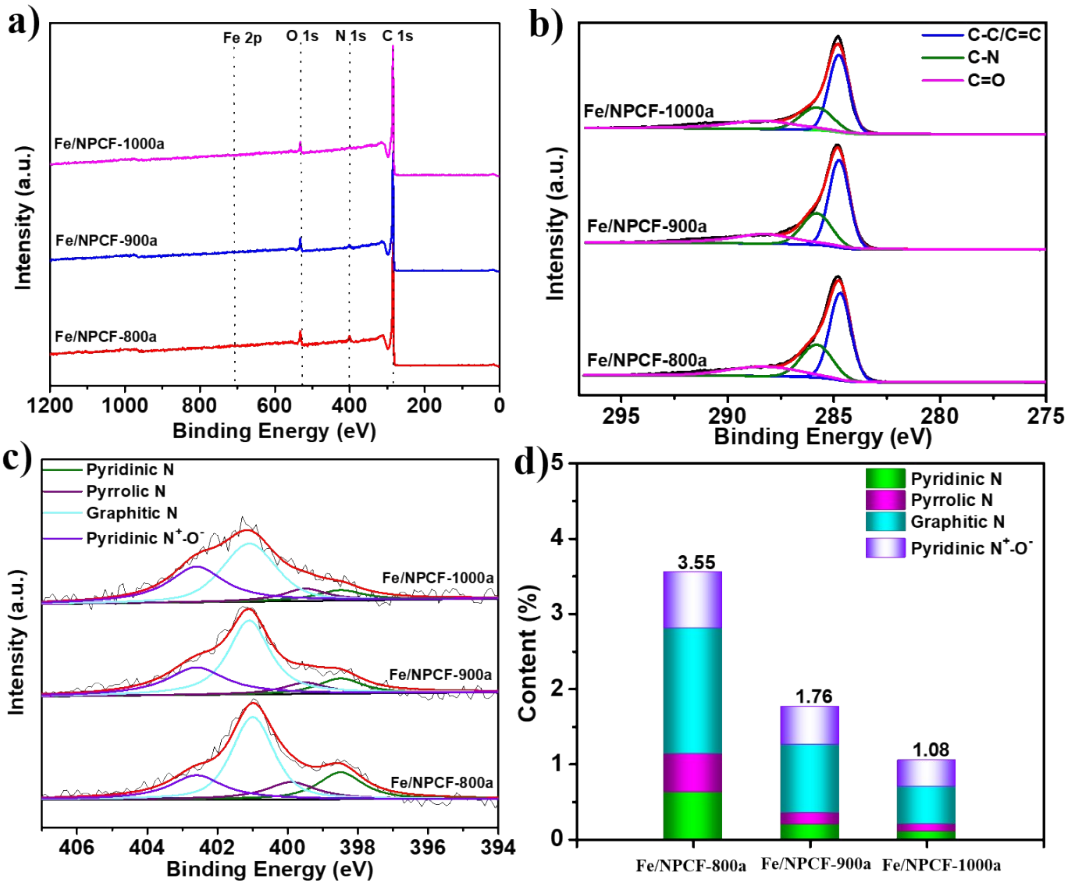

Figure S9. (a) XPS survey spectra; (b) High-resolution C 1s spectra; (c) High-resolution N 1s spectra; and (d) Corresponding nitrogen bonding configurations for Fe/NPCF-800a, Fe/NPCF-900a, and Fe/NPCF-1000a.

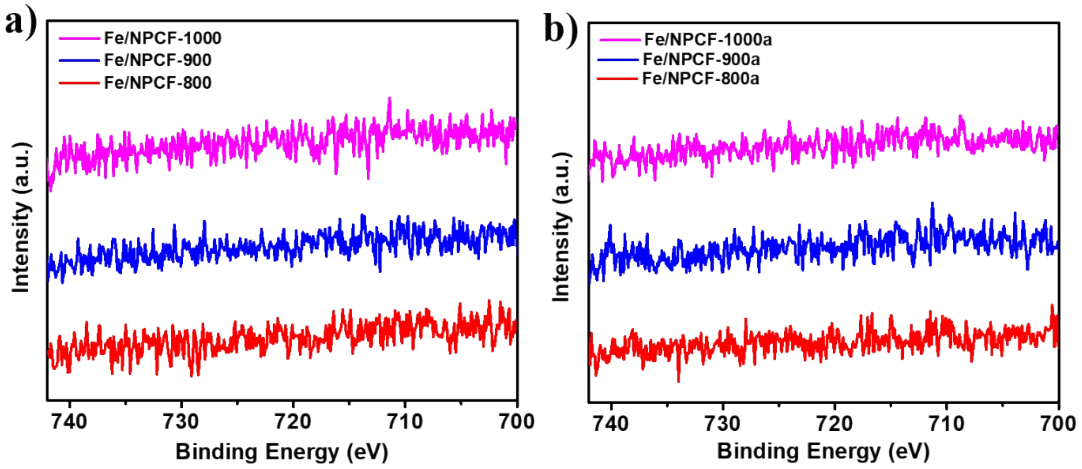

Figure S10. High-resolution of Fe 2p spectra of (a) Fe/NPCF-800, Fe/NPCF-900, and Fe/NPCF-1000; (b) Fe/NPCF-800a, Fe/NPCF-900a, and Fe/NPCF-1000a. No metal trace can be detected, indicating that most of Fe have been etched by the acidic etching process, and residual Fe in materials is below the detection limit.

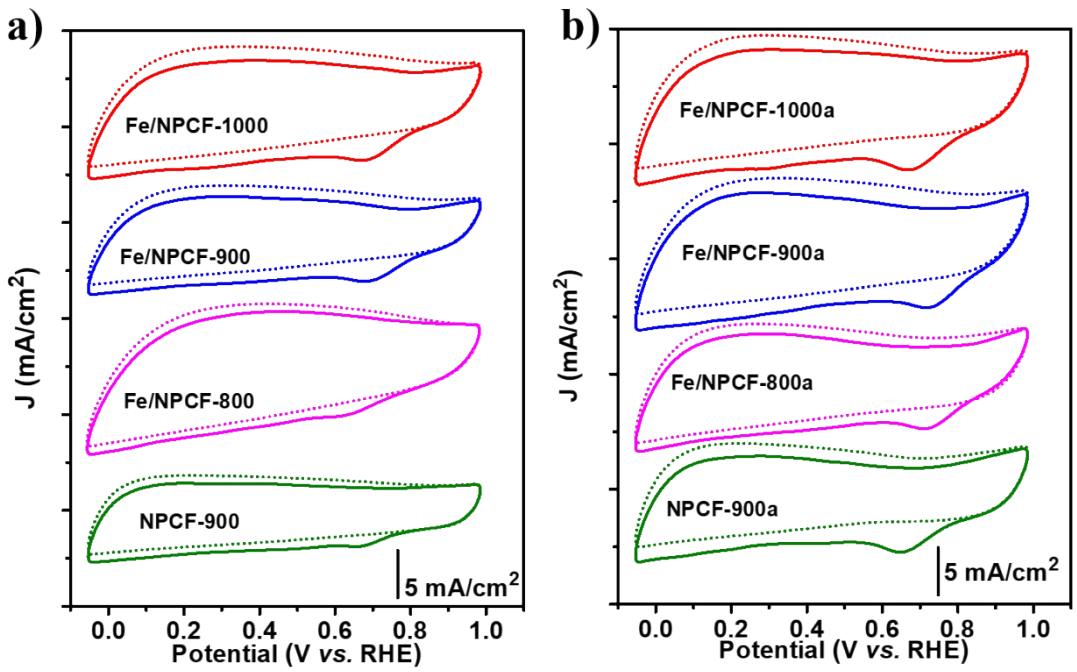

Figure S11. CV curves for Fe/NPCFs performed at N_2-saturated (dotted line) and O_2-saturated (solid line) 0.1 M KOH solution. It can be found that no redox features were discovered in N_2-saturated solution. By contrast, an obvious cathodic peak was detected in the case of O_2-saturated, suggesting the electrocatalytic activity for ORR.

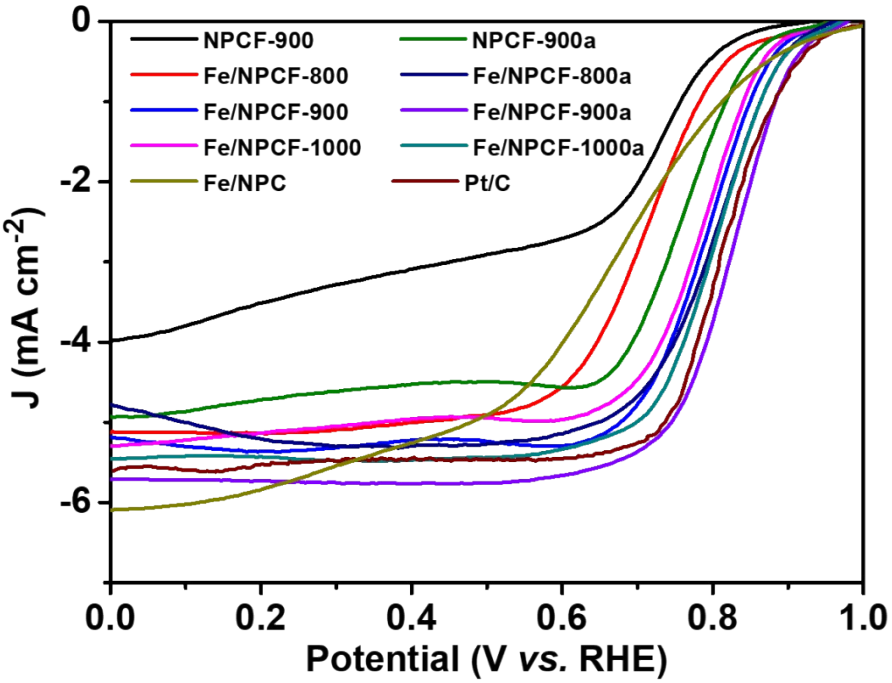

Figure S12. RDE polarization curves for as-prepared materials and commercial Pt/C at rotation speed of 1600 rpm. It can be seen that the Fe/NPCFs show better activities than that of Fe/NPC.

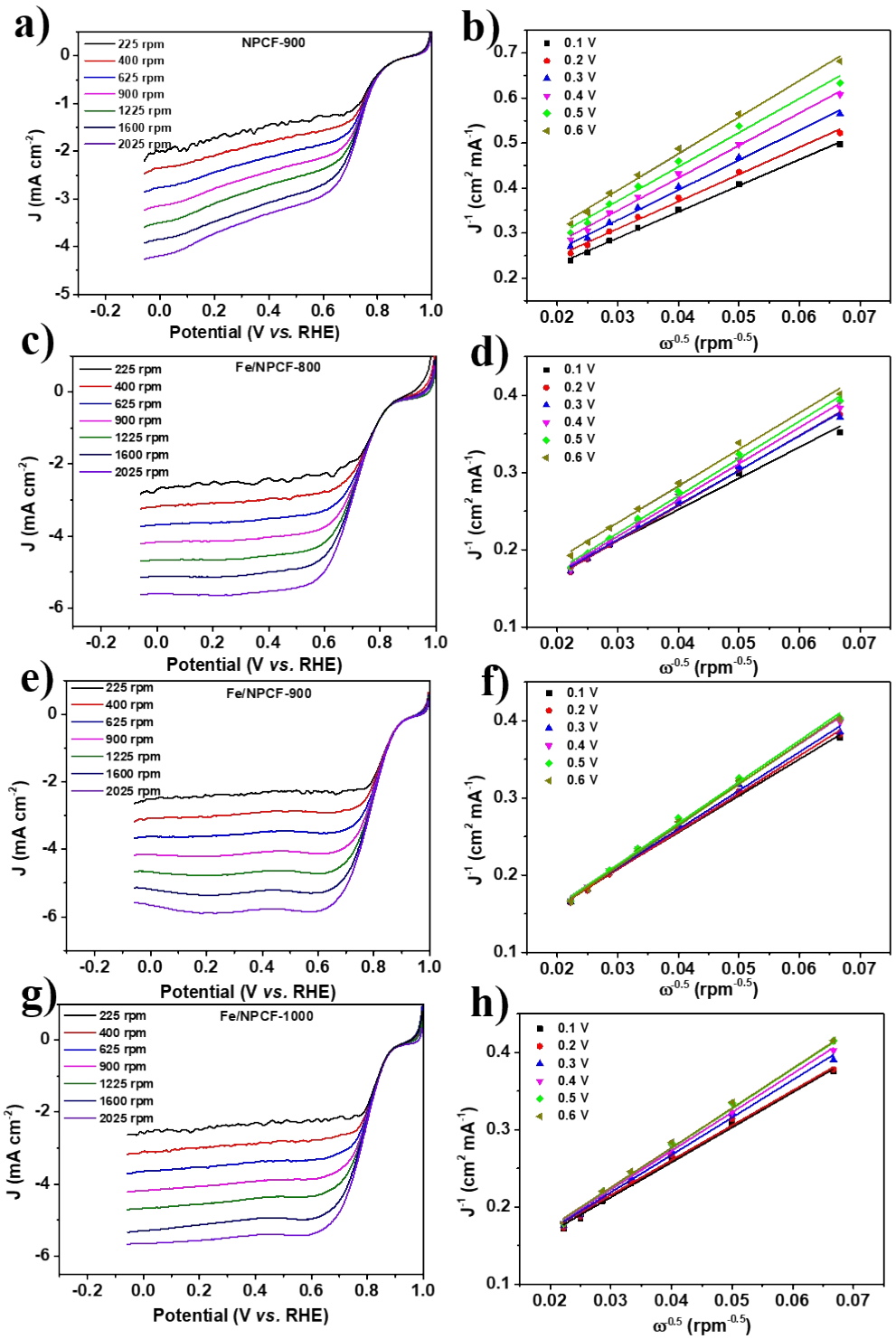

Figure S13. LSV curves of NPCF-900 (a), Fe/NPCF-800 (c), Fe/NPCF-900 (e) and Fe/NPCF-1000 (g) in oxygen-saturated 0.1 M KOH solution at different rotation rates. Figures (b), (d), (f) and (h) show the corresponding Koutecky–Levich plots at different potentials. Scan rate: 10 mVs^{-1}.

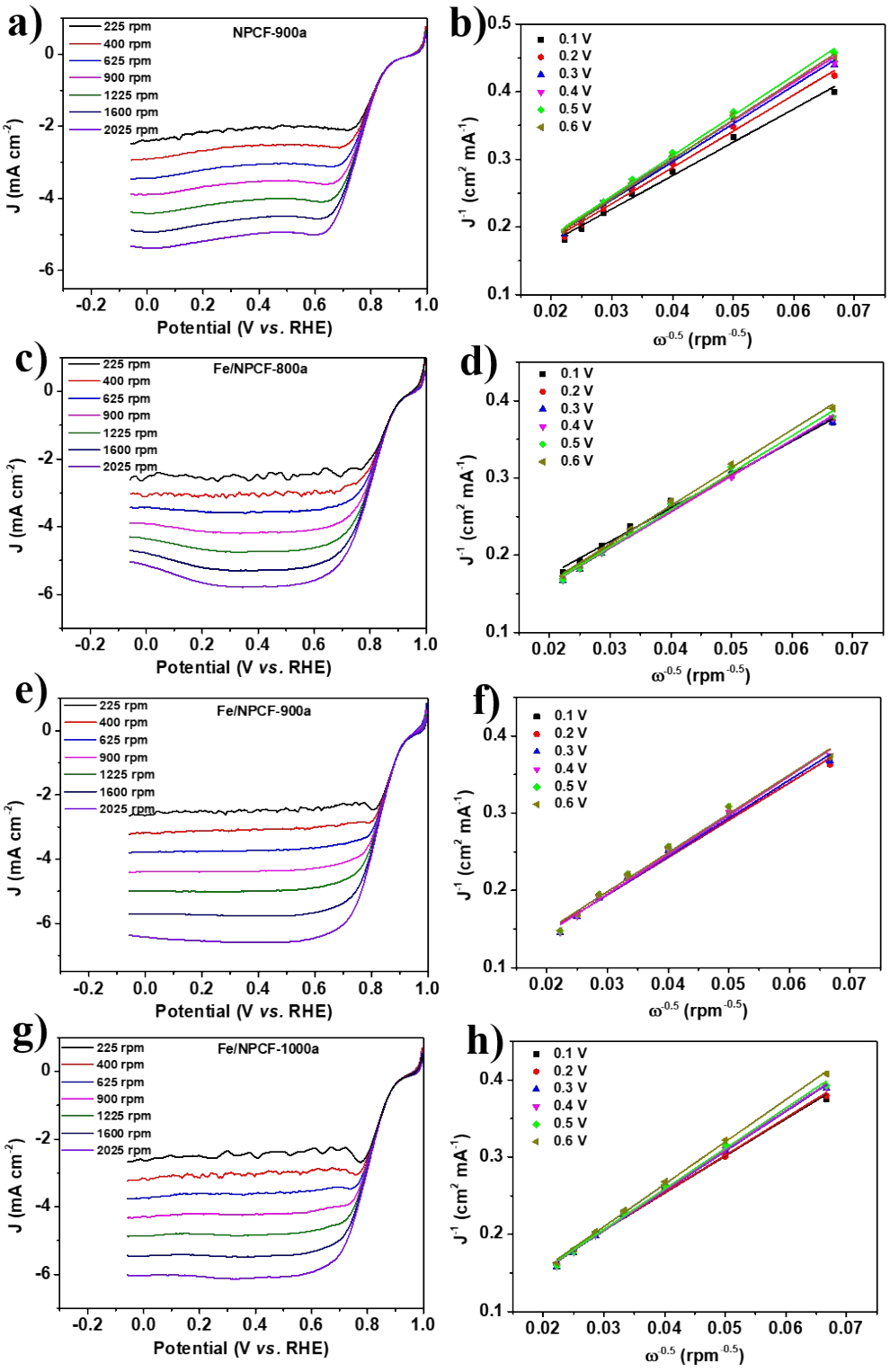

Figure S14. LSV curves of NPCF-900a (a), Fe/NPCF-800a (c), Fe/NPCF-900a (e) and Fe/NPCF-1000a (g) in O_2-saturated 0.1 M KOH solution at different rotation rates. Figures (b), (d), (f) and (h) show the corresponding Koutecky–Levich plots at different potentials. Scan rate: 10 mVs^{-1}.

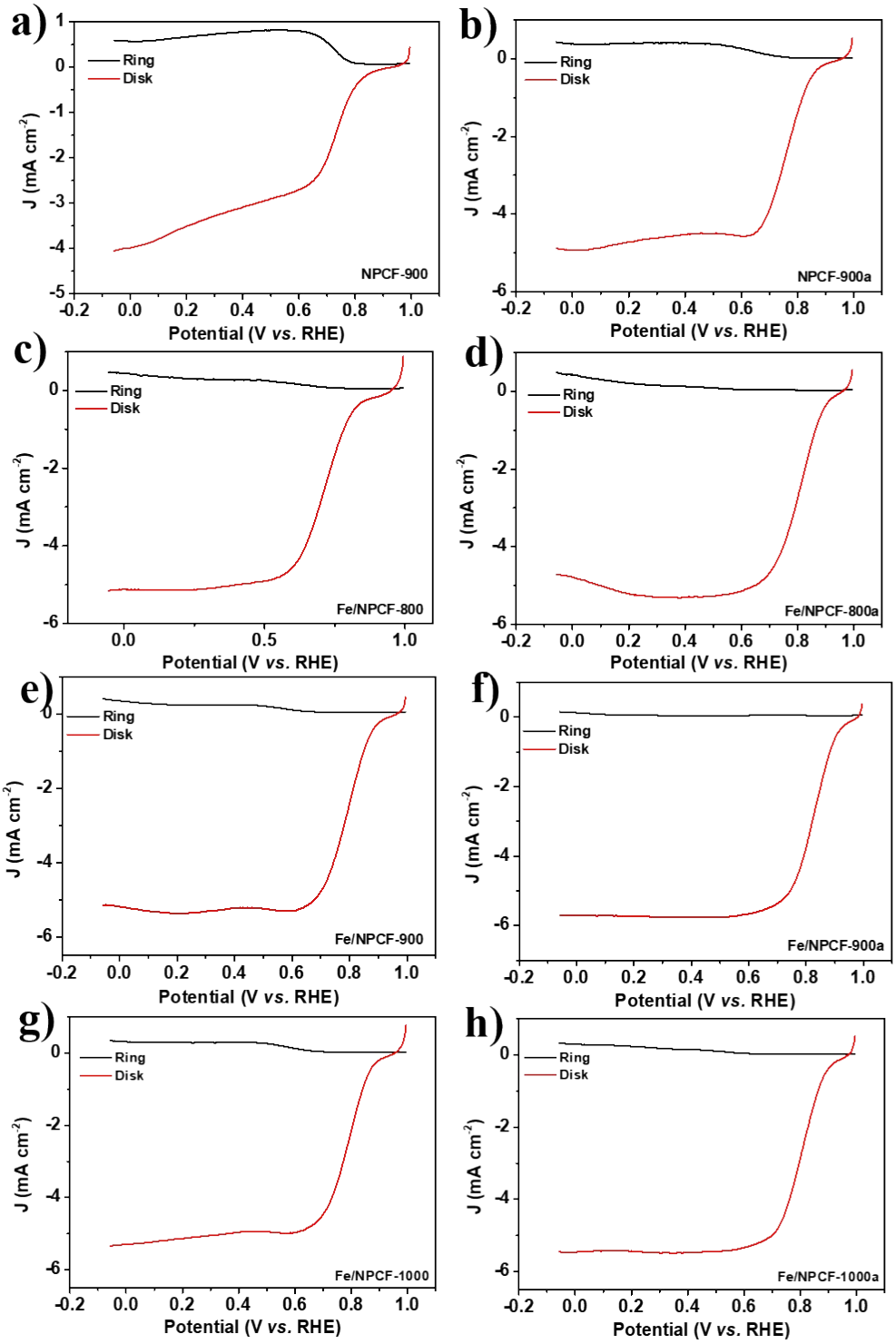

Figure S15. RRDE current−potential curves for NPCF-900 (a), NPCF-900a (b), Fe/NPCF-800 (c), Fe/NPCF-800a (d), Fe/NPCF-900 (e), Fe/NPCF-900a (f), Fe/NPCF-1000 (g), and Fe/NPCF-1000a (h) in O_2 saturated 0.1 M KOH solution. All samples were measured at an angular rotation rate of 1600 rpm.

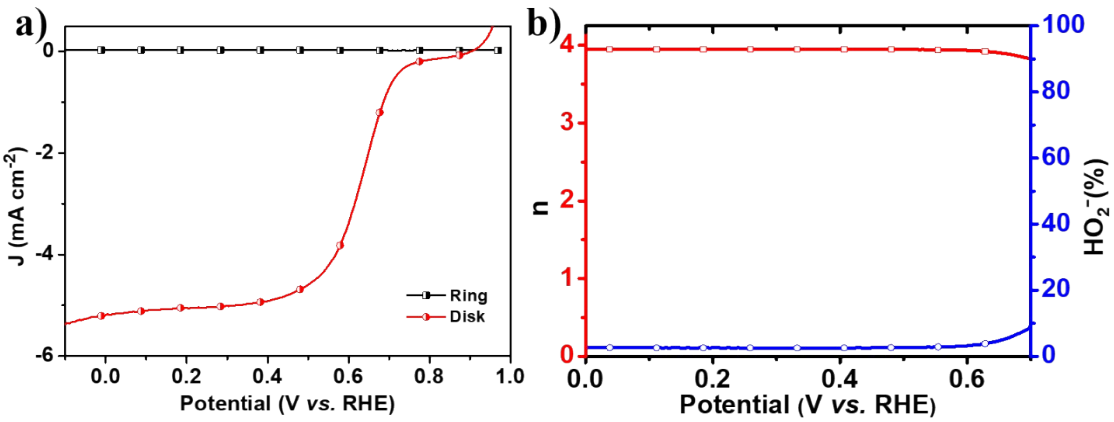

Figure S16. (a) RRDE current−potential curves for Fe/NPCF-900a in 0.5 M H_2SO_4 solution; (b) Corresponding electron-transfer number (n) and peroxide yield.

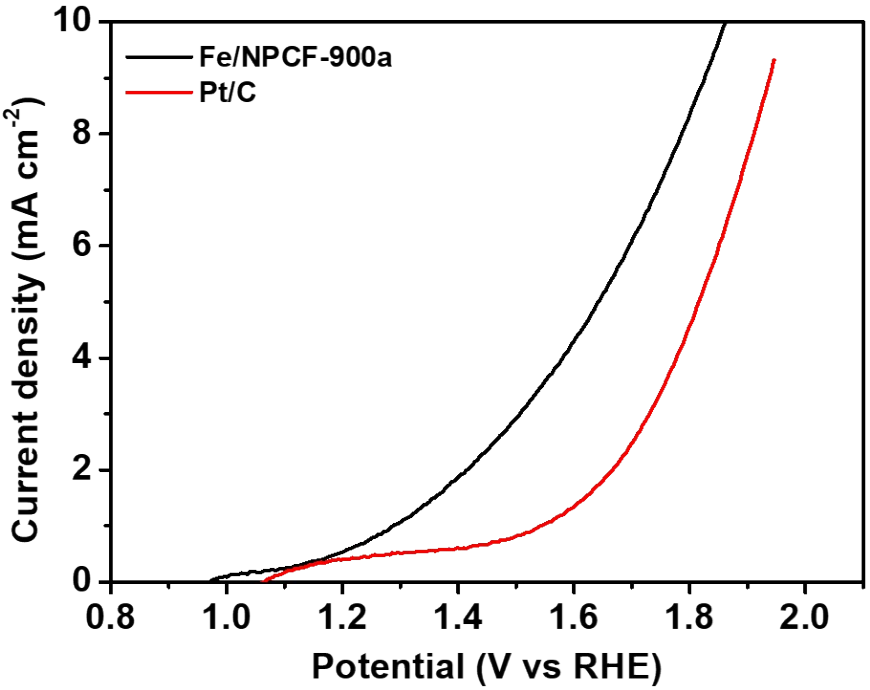

Figure S17. OER performance of Fe/NPCF-900a and Pt/C in 0.1 M KOH solution. Fe/NPCF-900a exhibit better activity than that of Pt/C.

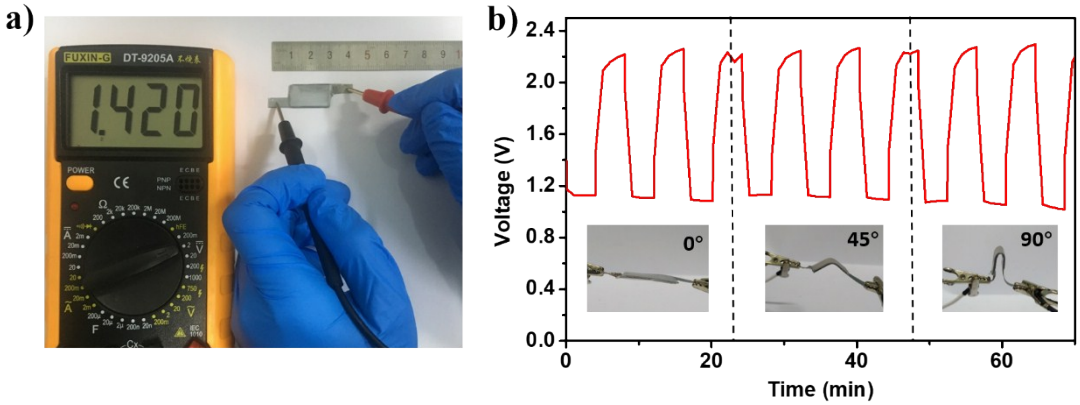

Figure S18. (a) Photograph of open-circuit voltage testing; (b) Blend batteries to different angles during charge and discharge testing. The open circuit voltage was measured to be 1.420 V. And as-fabricated battery can be bended to different angles, only a very slight voltage drops at the moment of bending battery to 45° and 90° during charge and discharge testing.

Table S1. Elemental analysis of obtained materials based on XPS analysis and ICP (wt.%)

Sample	C	N	Fe
Fe/NPCF-800	93.72	6.28	/
Fe/NPCF-900	96.43	3.57	/
Fe/NPCF-1000	98.17	1.83	/
Fe/NPCF-800a	96.45	3.55	0.21 by ICP
Fe/NPCF-900a	98.24	1.76	0.30 by ICP
Fe/NPCF-1000a	98.92	1.08	0.32 by ICP

Table S2. Comparison of ORR performance with reported iron doped carbon materials in 0.1 M KOH.

Catalysts	Onset potential (mV, vs RHE)	Half-wave potential (mV, vs RHE)	Limited current density (mA/cm^2)	Reference
C-FeHZ$_8$@g-C$_3$N$_4$	0.97	0.845	~5.40	[1]
NGM-CN-Fe	0.97	0.810	6.42	[2]
Fe-N-C HNSs	1.05	0.870	5.95	[3]
p-Fe-N-CNFs	0.91	0.820	5.51	[4]
Fe-N-DSC	1.03	0.84	4.50	[5]
Fe@C–NG/NCNTs	0.93	0.84	5.0	[6]
GL-Fe/Fe$_5$C$_2$/NG800	0.98	0.86	5.60	[7]
Fe0.3Co0.7/NC cages	0.98	0.88	6.1	[8]
COP-TPP(Fe)@MOF-900	~0.90	0.84	4.7	[9]
SA-Fe-HPC	/	0.89	5.4	[10]
Fe/Fe$_4$N@Pd/C	0.937	0.81	~5.2	[11]
1.5%Fe-N-GDY	0.94	0.83	5.4	[12]
FeSA-N-C	1.0	0.890	6.0	[13]
Co–Fe/NC-900	0.92	0.82	5.6	[14]
Fe–N–C	0.84	~0.60	3.8	[15]
NFe/CNs-700-800-NH$_3$	0.930	0.859	5.45	[16]
FeN$_2$/NOMC-3	/	0.863	~4.90	[17]
FeBNC-800	0.968	0.838	5.51	[18]
PpPD-Fe-C	0.826	0.718	~3.60	[19]
Fe-N-GC	0.970	0.85	4.5	[20]
Fe$_3$C/C-700	0.91	0.83	4.1	[21]
Fe-N/C-700	0.956	0.840	5.8	[22]
Fe-N-C	0.923	0.800	6.06	[23]
FeNxC/C–S	0.91	0.72	5.30	[24]
Fe/NPCF-900a	0.907	0.827	5.76	This work

Table S3. Comparison of ORR performance with reported nonprecious carbon based materials in acidic media.

Catalysts	Media	Half-wave potential (mV, vs RHE)	Limited current density (mA/cm^2)	Reference
C-FeHZ$_8$@g-C$_3$N$_4$	0.1 M $HClO_4$	0.78	5.4	[1]
p-Fe-N-CNFs	0.1 M $HClO_4$	0.74	5.5	[4]
Fe-N-DSC	0.5 M H_2SO_4	0.65	4.6	[5]
GL-Fe/Fe$_5$C$_2$/NG-800	0.5 M H_2SO_4	0.60	/	[7]
SA-Fe-HPC	0.1 M H_2SO_4	0.81	5.5	[10]
1.5%Fe-N-GDY	0.1 M $HClO_4$	~0.62	4.5	[12]
FeSA-N-C	0.1 M $HClO_4$	0.78	~5.7	[13]
Fe-N/C-700	0.1 M $HClO_4$	0.67	5.9	[22]
Fe$_2$-Z$_8$-C	0.5 M H_2SO_4	0.805	~5.5	[25]
N/Fe-CG	0.1 M $HClO_4$	0.73	5.1	[26]
(Fe,Co)/N-C	0.1 M $HClO_4$	0.863	~5.8	[27]
TriCB-Fe/N/S/C	0.1 M $HClO_4$	~0.78	5.1	[28]
Fe$_{14}$NDC-9-W$_{2M}$-9	0.1 M $HClO_4$	0.73	/	[29]
Fe/SNC	0.5 M H_2SO_4	0.77	4.3	[30]
FeNC-S-FexC/Fe	0.1 M $HClO_4$	0.82	5.8	[31]
FePPy-900	0.5 M H_2SO_4	0.74	5.7	[32]
Fe-N-C	0.1 M $HClO_4$	0.75	4.1	[33]
Co/N/C	0.1 M $HClO_4$	0.63	3.8	[34]
NPC-F	0.5 M H_2SO_4	0.66	4.7	[35]
N-OMC-1050	0.5 M H_2SO_4	0.62	3.7	[36]
N-F-CNFs-950	0.5 M H_2SO_4	0.61	5.5	[37]
F, N, S-rGO	0.5 M H_2SO_4	0.39	3.1	[38]
Fe/NPCF-900a	0.5 M H_2SO_4	0.632	5.1	This work

Table S4. Comparison of Zn-air batteries performance of this work with recently reported similar catalytic materials.

Catalysts	Peak power density ($mW\ cm^{-2}$)	Specific capacity ($mAh\ g^{-1}$)	Reference
NFe/CNs-700-800-NH_3	/	750	[16]
FeBNC-800	10.6	/	[18]
Fe−N/C−700	/	682	[22]
$Fe_{0.5}Co_{0.5}O_x$	86	756	[39]
Fe@N–C-700	220	/	[40]
N-GCNT/FeCo	89	872	[41]
Co_4N/CNW/CC	174	/	[42]
Co-NB-CSs	100.4	/	[43]
rGO–IL/Mn_3O_4	120	/	[44]
α-MnO_2/XC-72	61.5	/	[45]
Cu-Pt	/	560	[46]
Fe/NPCF-900a	158.5	717.8	This work

Reference:

1. Y. Deng, B. Chi, X. Tian, Z. Cui, E. Liu, Q. Jia, W. Fan, G. Wang, D. Dang, M. Li, K. Zang, J. Luo, Y. Hu, S. Liao, X. Sun and S. Mukerjee, *J. Mater. Chem. A*, 2019, **7**, 5020-5030.
2. C. Wang, H. Zhao, J. Wang, Z. Zhao, M. Cheng, X. Duan, Q. Zhang, J. Wang and J. Wang, *J. Mater. Chem. A*, 2019, **7**, 1451-1458.
3. Y. Chen, Z. Li, Y. Zhu, D. Sun, X. Liu, L. Xu and Y. Tang, *Adv. Mater.*, 2019, **31**, 1806312.
4. B.-C. Hu, Z.-Y. Wu, S.-Q. Chu, H.-W. Zhu, H.-W. Liang, J. Zhang and S.-H. Yu, *Energy Environ. Sci.*, 2018, **11**, 2208-2215.
5. Z. Huang, H. Pan, W. Yang, H. Zhou, N. Gao, C. Fu, S. Li, H. Li and Y. Kuang, *ACS Nano*, 2018, **12**, 208-216.
6. Q. Wang, Y. Lei, Z. Chen, N. Wu, Y. Wang, B. Wang and Y. Wang, *J. Mater. Chem. A*, 2018, **6**, 516-526.
7. E. Hu, X.-Y. Yu, F. Chen, Y. Wu, Y. Hu and X. W. Lou, *Adv. Energy Mater.,* 2018, **8**, 1702476.
8. B. Y. Guan, Y. Lu, Y. Wang, M. Wu and X. W. Lou, *Adv. Funct. Mater.*, 2018, **28**, 1706738.
9. J. Guo, Y. Li, Y. Cheng, L. Dai and Z. Xiang, *ACS Nano*, 2017, **11**, 8379-8386.
10. Z. Zhang, J. Sun, F. Wang and L. Dai, *Angew. Chem., Int. Ed.*, 2018, **130**, 9176-9181.
11. W. Jiao, C. Chen, W. You, J. Zhang, J. Liu and R. Che, *Small*, 2019, **15**, 1805032.
12. W. Si, Z. Yang, X. Wang, Q. Lv, F. Zhao, X. Li, J. He, Y. Long, J. Gao and C. Huang, *ChemSusChem*, 2019, **12**, 173-178.
13. L. Jiao, G. Wan, R. Zhang, H. Zhou, S.-H. Yu and H.-L. Jiang, *Angew. Chem., Int. Ed.*, 2018, **130**, 8661-8665.
14. S. L. Zhang, B. Y. Guan and X. W. Lou, *Small*, 2019, **15**, 1805324.
15. M. Sun, D. Davenport, H. Liu, J. Qu, M. Elimelech and J. Li, *J. Mater. Chem. A*, 2018, **6**, 2527-2539.
16. S. Li, C. Cheng, H.-W. Liang, X. Feng and A. Thomas, *Adv. Mater.*, 2017, **29**, 1700707.
17. H. Shen, E. Gracia-Espino, J. Ma, H. Tang, X. Mamat, T. Wagberg, G. Hu and S. Guo, *Nano Energy*, 2017, **35**, 9-16.
18. K. Yuan, S. Sfaelou, M. Qiu, D. Lützenkirchen-Hecht, X. Zhuang, Y. Chen, C. Yuan, X. Feng and U. Scherf, *ACS Energy Lett.*, 2018, **3**, 252-260.
19. Y. Zhu, B. Zhang, X. Liu, D.-W. Wang and D. S. Su, *Angew. Chem., Int. Ed.*, 2014, **53**, 10673-10677.
20. A. Kong, X. Zhu, Z. Han, Y. Yu, Y. Zhang, B. Dong and Y. Shan, *ACS Catal.*, 2014, **4**, 1793-1800.
21. Y. Hu, J. O. Jensen, W. Zhang, L. N. Cleemann, W. Xing, N. J. Bjerrum and Q. Li, *Angew. Chem. Int. Ed.,* 2014, **53**, 3675-3679.
22. Z. K. Yang, L. Lin and A.-W. Xu, *Small*, 2016, **12**, 5710-5719.
23. L. Lin, Q. Zhu and A.-W. Xu, *J. Am. Chem. Soc.*, 2014, **136**, 11027-11033.
24. J. Zhang, D. He, H. Su, X. Chen, M. Pan and S. Mu, *J. Mater. Chem. A*, 2014, **2**, 1242-1246.
25. Q. Liu, X. Liu, L. Zheng and J. Shui, *Angew. Chem., Int. Ed.*, 2018, **57**, 1204-1208.
26. B. Li, S. P. Sasikala, D. H. Kim, J. Bak, I.-D. Kim, E. Cho and S. O. Kim, *Nano Energy*, 2019, **56**, 524-530.
27. J. Wang, Z. Huang, W. Liu, C. Chang, H. Tang, Z. Li, W. Chen, C. Jia, T. Yao, S. Wei, Y. Wu and Y. Li, *J. Am. Chem. Soc.*, 2017, **139**, 17281-17284.

28. Y. Zhu, X. Chen, J. Liu, J. Zhang, D. Xu, W. Peng, Y. Li, G. Zhang, F. Zhang and X. Fan, *ChemSusChem*, 2018, **11**, 2402-2409.
29. M. Hoque, S. Zhang, M. L. Thomas, Z. Li, S. Suzuki, A. Ando, M. Yanagi, Y. Kobayashi, K. Dokko and M. Watanabe, *J. Mater. Chem. A*, 2018, **6**, 1138-1149.
30. H. Shen, E. Gracia-Espino, J. Ma, K. Zang, J. Luo, L. Wang, S. Gao, X. Mamat, G. Hu, T. Wagberg and S. Guo, *Angew. Chem., Int. Ed.*, 2017, **56**, 13800-13804.
31. Y. Qiao, P. Yuan, Y. Hu, J. Zhang, S. Mu, J. Zhou, H. Li, H. Xia, J. He and Q. Xu, *Adv. Mater.*, 2018, **30**, 1804504.
32. T.-N. Tran, M. Y. Song, K. P. Singh, D.-S. Yang and J.-S. Yu, *J. Mater. Chem. A*, 2016, **4**, 8645-8657.
33. M.-Q. Wang, W.-H. Yang, H.-H. Wang, C. Chen, Z.-Y. Zhou and S.-G. Sun, *ACS Catal.*, 2014, **4**, 3928-3936.
34. S. Ma, G. A. Goenaga, A. V. Call and D.-J. Liu, *Chem.–Eur. J.*, 2011, **17**, 2063-2067.
35. Z. Xu, X. Zhuang, C. Yang, J. Cao, Z. Yao, Y. Tang, J. Jiang, D. Wu and X. Feng, *Adv. Mater.*, 2016, **28**, 1981-1987.
36. X. Wang, J. S. Lee, Q. Zhu, J. Liu, Y. Wang and S. Dai, *Chem. Mater.*, 2010, **22**, 2178-2180.
37. L. Cao, X. Zhou, Z. Li, K. Su and B. Cheng, *J. Power Sources*, 2019, **413**, 376-383.
38. A. Zehtab Yazdi, E. P. L. Roberts and U. Sundararaj, *Carbon*, 2016, **100**, 99-108.
39. H.-F. Wang, C. Tang and Q. Zhang, *Adv. Funct. Mater.*, 2018, **28**, 1803329.
40. J. Wang, H. Wu, D. Gao, S. Miao, G. Wang and X. Bao, *Nano Energy*, 2015, **13**, 387-396.
41. C. Y. Su, H. Cheng, W. Li, Z. Q. Liu, N. Li, Z. Hou, F. Q. Bai, H. X. Zhang and T. Y. Ma, *Adv. Energy Mater.*, 2017, **7**, 1602420.
42. F. Meng, H. Zhong, D. Bao, J. Yan and X. Zhang, *J. Am. Chem. Soc.,* 2016, **138**, 10226-10231.
43. Y. Guo, P. Yuan, J. Zhang, Y. Hu, I. S. Amiinu, X. Wang, J. Zhou, H. Xia, Z. Song, Q. Xu and S. Mu, *ACS Nano*, 2018, **12**, 1894-1901.
44. J.-S. Lee, T. Lee, H.-K. Song, J. Cho and B.-S. Kim, *Energy Environ. Sci.*, 2011, **4**, 4148-4154.
45. Y. Dong and J. Li, *Chem. Commun.*, 2015, **51**, 572-575.
46. V. M. Dhavale and S. Kurungot, *ACS Catal.*, 2015, **5**, 1445-1452.